Steel and Composite Structures, *Vol. 33, No. 3* (*2019*) *433-444*
DOI: https://doi.org/10.12989/scs.2019.33.3.433

Variable amplitude fatigue test of M30 high-strength bolt in bolt-sphere joint grid structures

Bin Qiu [a], Honggang Lei*, Xu Yang, Zichun Zhou and Guoqing Wang

College of Civil Engineering, Taiyuan University of Technology, 79 West Yingze Street, Taiyuan, Shanxi, People's Repulic of China

(*Received April 25, 2019, Revised September 25, 2019, Accepted October 26, 2019*)

Abstract. Fatigue failure of a grid structure using bolt-sphere joints is liable to occur in a high-strength bolt due to the alternating and reciprocal actions of a suspension crane. In this study, variable amplitude fatigue tests were carried out on 20 40 Cr steel alloy M30 high-strength bolts using an MTS fatigue testing machine, and four cyclic stress amplitude loading patterns, Low-High, High-Low, Low-High-Low, and High-Low-High, were tested. The scanning electron microscope images of bolt fatigue failure due to variable amplitude stress were obtained, and the fractographic analysis of fatigue fractures was performed to investigate the fatigue failure mechanisms. Based on the available data from the constant amplitude fatigue tests, the variable amplitude fatigue life of an M30 high-strength bolt in a bolt-sphere joint was estimated using both Miner's rule and the Corten-Dolan model. Since both cumulative damage models gave similar predictions, Miner's rule is suggested for estimating the variable-amplitude fatigue life of M30 high-strength bolts in a grid structure with bolt-sphere joints; the S-N fatigue curve of the M30 high-strength bolts under variable amplitude loading was derived using equivalent stress amplitude as a design parameter.

Keywords: grid structure; bolt-sphere joint; M30 high-strength bolt; variable amplitude fatigue; cumulative fatigue damage; S-N curve

1. Introduction

The bolt-sphere joint (Fig. 1) originated as the node in the German Mero system. Space frame grid structures with such joints are widely used in public and industrial buildings due to their tensile strength, rigidity, light weight, and ease of construction on site. Suspension cranes are often installed on space frame grids in factories, as shown in Fig. 2. However, metal fatigue is extremely likely to damage the grid structure due to the alternating and reciprocal actions of suspension cranes. It has been found that the failure of grid structures with bolt-sphere joints due to metal fatigue is liable to occur in high-strength bolts because of stress concentration and the notch effect as dominant damage factors in grid structures with such joints (Lei and Yin 2008). As space frame roof structures that support suspension cranes have become more widely used in industrial buildings, the need to address the problem of fatigue in high-strength bolts in bolt-sphere joints has become more urgent.

Appendix 3 of *ANSI/AISC 360-16* (2010) states that no further evaluation of fatigue resistance is required when the cyclic applied stress range is less than the threshold of the allowable stress range. However, no calculation method is suitable for the fatigue design of a grid structure with bolt-sphere joints in Table A-3.1. Part 1.9 of the current

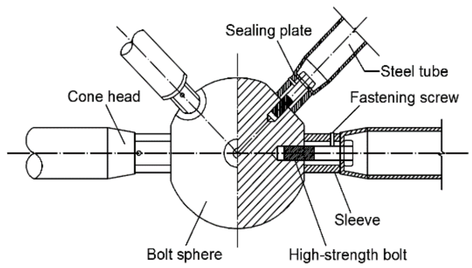

Fig. 1 Bolt-sphere joint

Fig. 2 An industrial plant with suspension crane

Eurocode 3 (2003) states that no provisions contained in Table 8.1 or Table 8.5 can be directly used for bolt-sphere joints and fatigue tests must be carried out to determine the fatigue strength for designs not included in the code. The current Chinese standard for the design of steel structures (GB50017-2017 2017) states that fatigue should be calculated for a steel member or its connectors under repeated dynamic loads of at least 5×10^4 cycles. However, bolt-sphere joints are not included in Appendix K for

*Corresponding author, Professor,
E-mail: lhgang168@126.com
[a] Ph.D., E-mail: tyutqbin@126.com

http://www.techno-press.org/?journal=scs&subpage=6
ISSN: 1229-9367 (Print), 1598-6233 (Online)

fatigue design. The current Chinese technical specification for space frame structures (JGJ7-2010 2010) also states that fatigue in a grid structure that supports a suspension crane should be evaluated when the number of stress cycles exceeds 5×10^4. The allowable stress range and acceptable design should be determined by a special fatigue test.

Available research into the fatigue of high-strength bolts in a grid structure using bolt-sphere joints is directed towards constant amplitude loading. Xu and Cui (1994) derived the S-N fatigue curves for M14 high-strength bolts commonly used in space frames, by conducting constant amplitude fatigue tests. Feng *et al.* (1995) established the S-N fatigue curve and the fatigue calculation method of M24 and M33 high-strength bolts in grid structures. Yang and Lei (2017) determined the S-N fatigue curves of M20 and M30 high-strength bolts used in a grid structure by conducting constant amplitude fatigue tests and studying the fatigue failure mechanism using metallographic analysis. Qiu *et al.* (2017) showed that the constant amplitude fatigue life of M30 high-strength bolts decreased greatly when the bolt was screwed into sphere to a depth of three threads. However, in practice, the engineering components are expected to experience variable amplitude loading over a period of time. Sunder (1979) derived a mathematical model of fatigue crack propagation under variable amplitude loading using the data obtained from constant amplitude loading and various loading sequences, such as High-Low or Low-High. He *et al.* (2018) investigated the effect of high-amplitude loading on accumulated fatigue damage in 316 stainless steel by performing fatigue tests on a grid as the subject to variable amplitude stress. Sarkar *et al.* (2019) investigated the failure modes and cumulative fatigue of laser-based powder bed fusion-produced stainless steel parts subject to variable amplitude loading.

In the calculation of fatigue life, Ibrahim and Pettit (2005) calculated fatigue life in metal and composite joints by investigating bolt joint constraint parameters. Using the degree of equivalent damage principle for multilevel amplitude loads or random amplitude loads, Zhu (2011) derived a model for the equivalent stress amplitude range using Miner's rule and the Corten-Dolan model. Ferjaoui *et al.* (2015) developed a model for the nucleation of fretting fatigue cracks in double-lap bolted joints based on the mechanics of continuous damage propagation, and the cumulative fatigue predicted by the model agreed well with experimental data. Zhou *et al.* (2015) constructed an equivalent stress model to investigate the multiaxial fatigue of a composite bolt joint under cyclic constant amplitude loading which gave predictions agreeing with experimental results. Zuo *et al.* (2015) developed a nonlinear cumulative damage model to predict fatigue life under variable amplitude loading which they validated experimentally. Kapidžić *et al.* (2016) investigated fatigue failure in carbon fiber reinforced polymer composites subject to double axial variable amplitude loading at high temperatures and developed a fatigue prediction model based on the mechanics of fractures.

The preceding review shows that the research into fatigue in high-strength bolts in space frame grids using bolt-sphere joints focuses on constant amplitude fatigue and that it is mostly undertaken in China. There are relatively few studies of the effects of variable amplitude fatigue on high-strength bolts in space frame grids that use bolt-sphere joints. Furthermore, there are no specific provisions for fatigue-resistant design of bolt-sphere joints in grid structures in current steel design specifications, whereby it suggests that experimental verification should be performed. This restricts the use of space frame grids in industrial plants, especially in large-scale buildings. Thus, it is essential to further investigate the fatigue performance of such joints. In this study, we conducted both experimental and theoretical analysis of fatigue in M30 high-strength bolts widely used in space frame grids with bolt-sphere joints, under variable amplitude loading. Thus, a method was developed to give a reasonable prediction of fatigue life.

Fig. 3 High-strength bolt specimens

(a) Bolt sphere

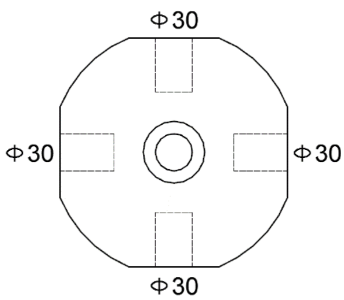

(b) Schematic diagram of bolt sphere

Fig. 4 Bolt sphere specimen

Table 1 Chemical composition (weight %) of M30 high-strength bolts

Name	C	Si	Mn	Cr	P	S
Bolt specimen	0.423	0.229	0.601	0.912	0.014	0.007
Standard value	0.37–0.44	0.17–0.37	0.50–0.80	0.80–1.10	≤ 0.035	≤ 0.035

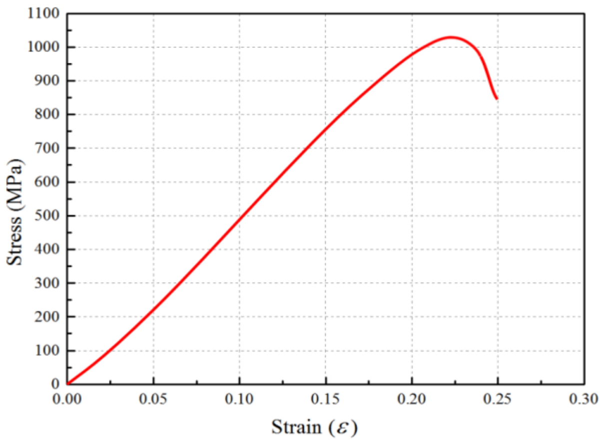

Fig. 5 The stress-strain curve of M30 high-strength bolt

2. Experimental methods

2.1 Specimen design

2.1.1 M30 high-strength bolt (30 mm nominal diameter)

The high-strength bolts (Fig. 3) used in the fatigue test are identical to those used in space frame grids. They are made of 40Cr steel alloy with a performance rating of 10.9S, produced in China. The appearance of each bolt was checked before the fatigue test, when those showing defects, such as cracks, rusts or bumps, were not used for the experiment. Each bolt was numbered.

2.1.2 BS200 bolt sphere (diameter 200 mm)

The bolt spheres (Fig. 4(a)) were made of 45# steel and were manufactured according to the provisions of *Bolted Spherical Node of Space Grid Structures* (JG/T 10:2009 2009). It was rather likely that during fatigue testing the bolt thread would be damaged or broken and that part or all of the bolt remained in the hole and could not be removed. To make the most use of the bolt spheres, three pairs of threads were set as a group (Φ30-Φ30) in each sphere, as shown in Fig. 4(b). If a thread failed, the fatigue test could still continue by changing the orientation of the sphere.

2.2 Material properties

The chemical composition of the bolts was determined (Table 1) and compared with the chemical composition requirements for 40Cr structural steel specified by *Carbon Structural Steel* (GB/T 700:2006 2006). Table 1 shows that the bolts meet the required standard.

Table 2 Mechanical properties of M30 high-strength bolts

Bolt	$\sigma_{0.2}$	$\bar{\sigma}_{0.2}$	σ_b	$\bar{\sigma}_b$	$\delta(\%)$	$\psi(\%)$
M30-a	973.5		1054.4			
M30-b	1032.1	998.5	1091.7	1067.7	10.3	42
M30-c	989.8		1056.9			

*Note. $\sigma_{0.2}$: conditional yield strength (MPa);
$\bar{\sigma}_{0.2}$: average value of conditional yield strength (MPa);
σ_b: ultimate tensile strength (MPa);
$\bar{\sigma}_b$: average value of ultimate tensile strength (MPa);
δ: elongation rate; ψ: shrinkage rate

The mechanical properties of the bolts were obtained from tensile tests of three randomly-selected specimen bolts using a WAW-2000 electro-hydraulic servo universal testing machine. The test results are given in Table 2, and the stress-strain curve of M30 high-strength bolts under static load is shown in Fig. 5, which shows that the bolts meet the requirements of *Bolted Spherical Node of Space Grid Structures* (JG/T 10:2009 2009). These properties were then used to determine the appropriate loading levels in variable amplitude fatigue testing.

2.3 Testing program and procedure

The variable amplitude fatigue tests were performed using the MTS Landmark 370.50 hydraulic servo fatigue test machine (MTS) which had a 500 kN capacity. In practice, the joints are subjected to concurrent loading from all the bolts, which makes the state of loading multiaxial and more complex; interaction between the different loadings can significantly affect fatigue life. Some simplifications were made in the testing: only axial tension loading was tested; the steel pipes and sealing plate connectors were removed; the head of each bolt was directly clamped to the fixture of the MTS to conduct the variable amplitude fatigue test. The fatigue loading test configuration is shown in Fig. 6. According to the ASTM standard *Test Method for Strain-Controlled Fatigue Testing* (ASTM E606/E606M-12 2012) and the Chinese standard

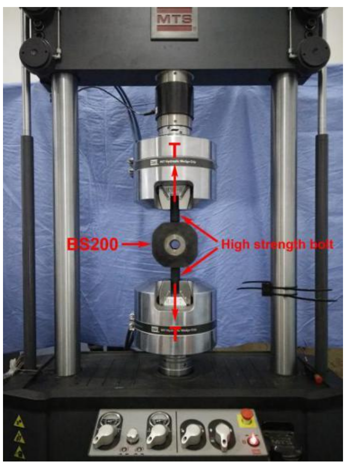

Fig. 6 A general view of the fatigue loading test

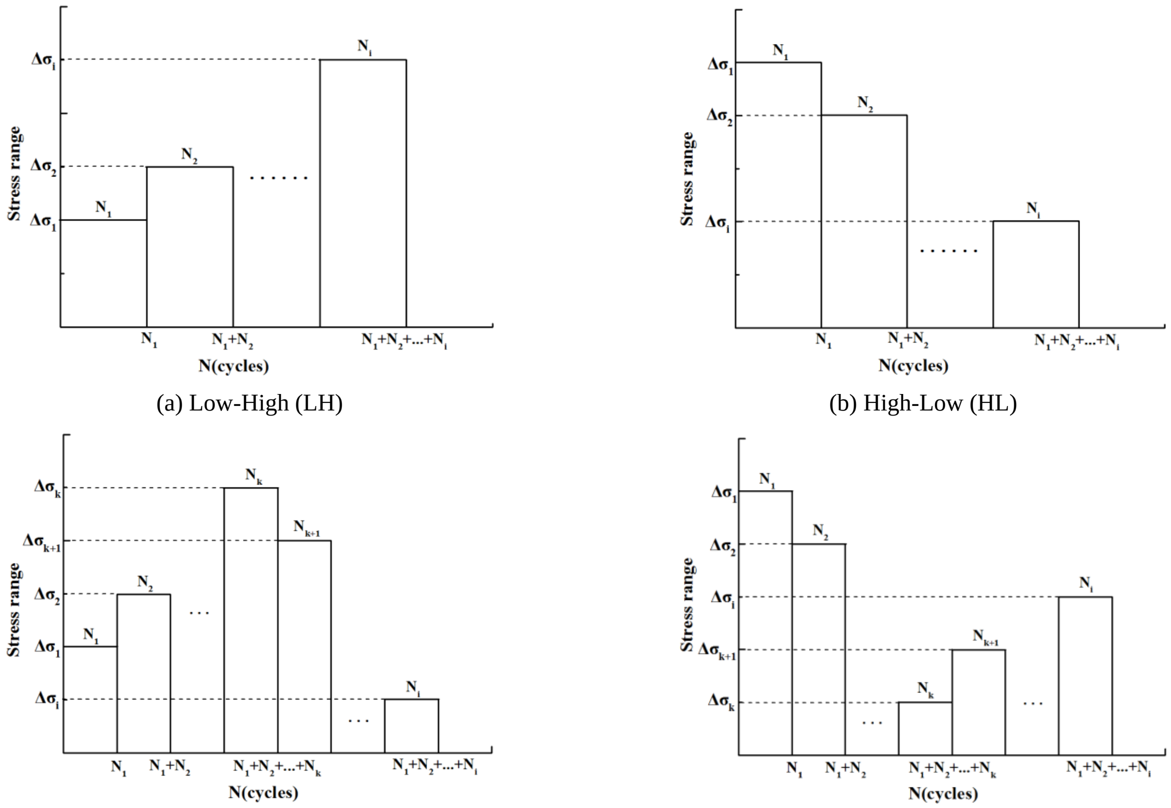

(a) Low-High (LH) (b) High-Low (HL)

(c) Low-High-Low (LHL) (d) High-Low-High (HLH)

Fig. 7 Stress histograms of the four loading patterns

Axial Load Fatigue Testing for Threaded Fasteners (GB/T13682-1992 1992), and considering the condition of the test equipment and the test period, the tests were performed with a cyclic sinusoidal loading at 7 Hz. Since the stress ratio of a lower chord is generally > 0.5 in a bolt-sphere joint grid structure with suspension cranes (Feng 2017), we set the stress ratio R ($R = \sigma_{max}/\sigma_{min}$) to 0.6. The loading levels of the tests were determined by the yield strength of the specimens (Table 2). The maximum stress (σ_{max}) of each loading step was set from $0.2f_y$ to $0.6f_y$ to maintain the specimens at an elastic state throughout the experiment. The minimum stress (σ_{min}) was obtained using the stress ratio. The stress was calculated as $\sigma = P/A_{eff}$, where P is the axial tension load, A_{eff} is the effective area of the bolt, and $\Delta\sigma = \sigma min_{max}$ was the stress range.

A load spectrum should be used in a fatigue test of bolt-sphere joints because the repeated loads on the grid structure generated by suspension cranes are random and complex. However, a generally accepted standard fatigue load spectrum has not yet been developed, due to limited research. Thus, we used a simplified fatigue load spectrum that reflected observed random loads. The variable amplitude loads consisted of four loading patterns: Low-High (LH), High-Low (HL), Low-High-Low (LHL) and High-Low-High (HLH), as shown in Fig. 7. Each load pattern included two or more stages of constant amplitude loading. In LH, a previous step had a lower stress amplitude than a later step, whereas in HL a previous step had a higher stress amplitude than a subsequent step. In LHL the loading pattern was from a low stress amplitude to a higher stress amplitude to a lower stress amplitude, whereas in HLH the loading pattern was from a high stress amplitude to a lower stress amplitude to a higher stress amplitude. In each pattern, the load was applied until complete failure of the specimen. The number of cycles under a certain stress amplitude $\Delta\sigma_i$ was recorded as N_i, and the variable amplitude fatigue life of each specimen tested was calculated as $N_f (N_f = N_1 + N_2 + \ldots N_i)$.

3. Results and discussion

3.1 Fatigue test results

In total, 20 satisfactory variable amplitude fatigue tests of the M30 high-strength bolts were conducted. The fatigue test results are given in Appendix A, Table A1, when the stress histograms of variable amplitude fatigue are shown in Fig. 8. Eight bolts (LH-1 to LH-8) were tested in LH; eight bolts (HL-1 to HL-8) were tested in HL; two bolts (LHL-1, LHL-2) were tested in LHL, and two bolts (HLH-1, HLH-2) were tested in HLH.

3.2 Fatigue test failures

Fig. 9 shows that fatigue failure of one high-strength bolt (HL-1) occurred in the first engaged thread between bolt and sphere, as a typical form of failure in bolt-sphere joints observed during the fatigue tests. All the bolt specimens displayed a fatigue failure similar to that of HL-

1. The reasons for such failures are:
   (1) The bolts are notched members; the stress concentration and notch effect at the threads are significant, and the effective cross-section at the threads is minimal. The part of the thread screwed into the sphere by 1.1d depth is engaged with the internal thread of the sphere, forming a load-bearing combination. However, the unmeshed parts of the thread on the bolts also bear load, whereby fatigue cracks are prone to occur there.
   (2) Errors during manufacturing and machining processes are unavoidable, whereby the axes of the bolts may not exactly match those of the threaded holes. Moreover, initial eccentricities might occur when the specimens are installed in the testing machine, causing a large bending stress concentrated at the first engaged thread. Therefore, fatigue failure of the bolt sphere joints is likely to occur at the first engaged thread at the meshing of bolt and sphere.

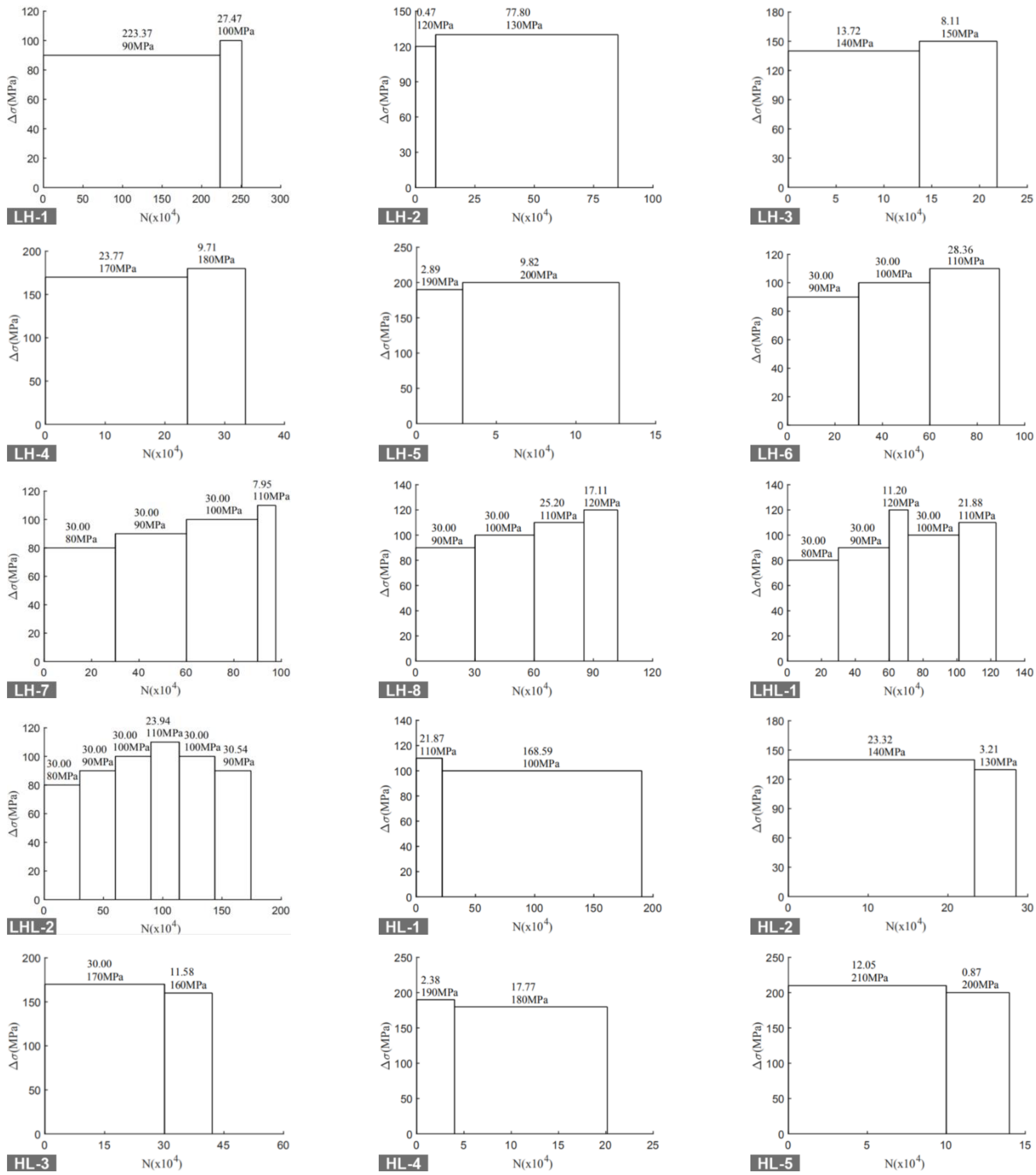

Fig. 8 The stress histogram of M30 high-strength bolts under variable amplitude loading

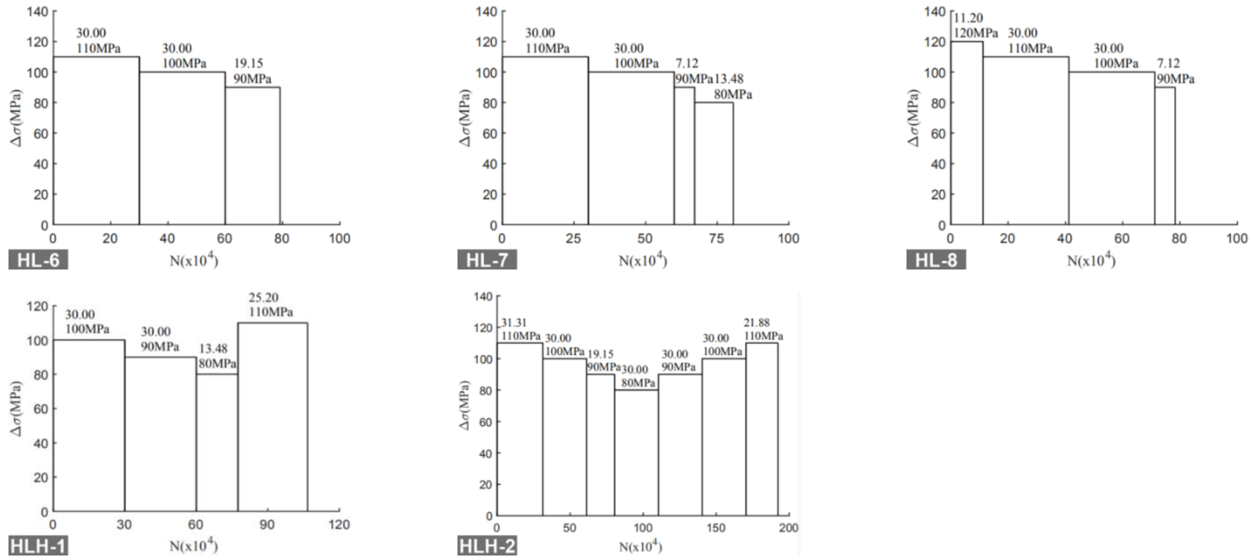

Fig. 8 Continued

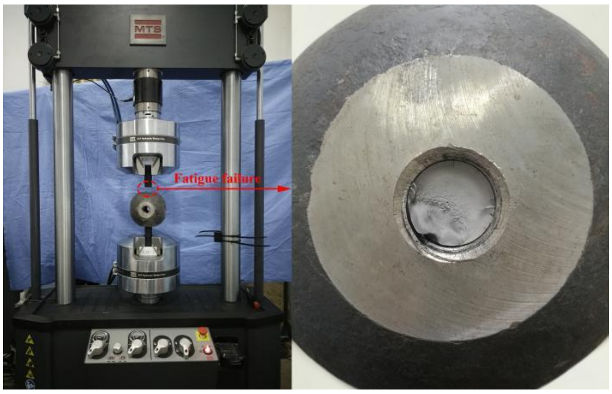

Fig. 9 Typical fatigue failure form of specimens

3.3 Fatigue damage and S-N curve

Fatigue damage models predict the service life of components or structures according to service conditions. If the fatigue life(N_f) of a component under stress is known, then the rest of the service life can be calculated, within a certain safety margin, using a fatigue damage model. We used Miner's rule (Miner 1945) and the Corten–Dolan model (Corten and Dolan 1956) to calculate the fatigue life of the M30 high-strength bolts under variable-amplitude stress.

3.3.1 Miner's Rule

Miner's rule is that the degree of fatigue damage is proportional to the number of loading cycles. It is expressed as

$$D_M = \sum_{i=1}^{i} \frac{n_i}{N_i} \tag{1}$$

where D_M is the total fatigue damage and n_i and N_i are respectively the numbers of loading cycles and fatigue life at the i^{th} loading cycle with stress amplitude $\Delta\sigma_i$. The subscript i is the loading sequence number. Miner's rule states that fatigue fracture occurs when $D_M = 1.0$. However, Miner's rule ignores the effects of the loading sequence, the interval time, and the interactions between different load levels on fatigue life.

3.3.2 Corten–Dolan model

The Corten–Dolan model is a modified linear cumulative damage model, in which the total number of cycles to failure (N_f) under multi-level loading blocks is calculated by

$$N_f = \frac{N_1}{\sum \alpha_i (\sigma_i/\sigma_{max})^d} \tag{2}$$

where $N_1$is the number of cycles to failure at the maximum stress loading σ_{max}, σ_i is the i^{th} level stress loading ($i = 1, 2, 3 \ldots.$), n_i is the number of stress loading cycles corresponding to σ_i, α_i is the proportion of cyclic stress σ_i, and d is a material constant derived from the experimental data. On the basis of fatigue test data, Corten and Dolan (1956) recommended that $d = 4.8$ for high-strength steel and $d = 5.8$ for other steels. Substituting $d = 4.8$ into Eq. (2), the total fatigue damage D_{CD} can be calculated by

$$D_{CD} = \sum_{i=1}^{i} \frac{\alpha_i N_f}{N_1 (\sigma_{max}/\sigma_i)^d} \tag{3}$$

We analyzed data for 37 completed constant-amplitude fatigue tests (Appendix B, Table B1) to calculate the variable amplitude fatigue damage of the M30 high-strength bolts, and used the S-N fatigue curve equation for 95% survival probability (Yang 2017)

$$log_{10} N = 12.221 - 3.087\, log_{10}(\Delta\sigma) \\ -1.645 \times 0.155 \tag{4}$$

$$\begin{aligned} r &= -0.949, \\ [\Delta\sigma]_{2\times10^6} &= 68.41\ MPa \end{aligned} \tag{4}$$

where r is the correlation coefficient and $[\Delta\sigma]_{2\times10^6}$ is the allowable maximum nominal stress range corresponding to 2×10^6 cycles with 95% survival probability. Based on the constant-amplitude fatigue test results for the bolts, the results of the variable amplitude fatigue damage calculations are given in Table 3.

Table 3 shows that the values of total fatigue damage D, calculated by two models under variable amplitude loading, were scattered. We explain this by noting that the assumptions of cumulative damage theory do not represent the loading conditions of the tests we conducted. For example, all fatigue test loading programs were in a tension–tension cycle, and the mean stress of each cycle is much greater than 0. The maximum and minimum values of D_M are 0.602 and 1.829, and the maximum and minimum values of D_{CD} are 0.564 and 1.785. A comparison between the values of D_M and D_{CD} shows some differences between the two sets of results, but both of them give similar predictions. In general, the fatigue damage values D calculated by the two models are acceptable, except for a few specimens, particularly HL-3 and LH-3. The D value for HL-3 is much greater than 1.0 while that for LH-3 is much less than 1.0. We offer the following as possible causes: (1) different stress loading conditions cause nonuniform damage to the bolts at the same stress level; (2) an inevitable breakdown of the test machine forces the replacement of the specimen, thus interrupting the test; (3) an effect caused by the treatment of the thread surface during bolt manufacture. The loading patterns for specimens LH-1 and HL-1 were different, but the mean stress ranges which they experienced in the tests were relatively low. In this case, the low stress cycles could increase fatigue strength due to strain hardening of the material, resulting in the cumulative damage D values for these two specimens being greater than for other specimens.

According to Miner's rule, the formula for calculating the equivalent stress amplitude of the M30 high-strength bolts under variable amplitude loading conditions is given by (Chen 2016)

$$\Delta\sigma_e = \left(\sum_{i=1}^{i} f_i \cdot \Delta\sigma_i{}^m\right)^{1/m} \tag{5}$$

where $\Delta\sigma_e$ is the equivalent stress amplitude, $\Delta\sigma_i$ is the i^{th} level stress amplitude, f_i is the cyclic stress frequency $\Delta\sigma_i$, m is an empirically-determined constant, derived from the constant-amplitude fatigue test S-N curve, as shown in Eq. (4), m = 3.087 is obtained. The corresponding fatigue design curve of constant amplitude fatigue test data is shown in Fig. 10 for comparison with the calculation results of equivalent stress amplitude calculation using Miner's rule. The fatigue S-N curve equation with equivalent stress amplitude as parameter under the 95% survival probability is

$$\begin{aligned} log_{10}\,N &= 11.664 - 2.814\,log_{10}(\Delta\sigma_e) \\ &\quad -1.645\times0.163 \\ r &= -0.901, \\ [\Delta\sigma]_{2\times10^6} &= 64.65MPa \end{aligned} \tag{6}$$

The slope of the equivalent stress amplitude S-N curve was slightly less steep than that of the constant amplitude data curve, and the allowable maximum equivalent stress range corresponding to 2×10^6 loading cycles under the 95% survival probability was 64.65 MPa, which was 5.8% lower than the constant amplitude fatigue test results.

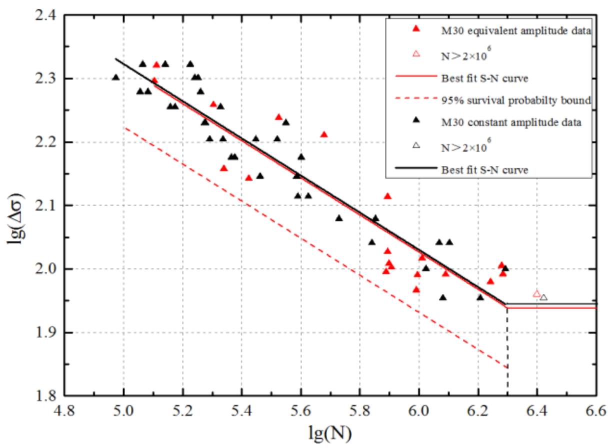

Fig. 10 Double logarithm regression curve with $lg\,\Delta\,\sigma$ as the parameter

Table 3 Results of cumulative fatigue damage based on the two models

Specimen number	Total fatigue damage, D		Specimen number	Total fatigue damage, D	
	D_M	D_{CD}		D_M	D_{CD}
LH-1	1.695	1.455	HL-1	1.776	1.548
LH-2	1.642	1.576	HL-2	0.656	0.648
LH-3	0.602	0.564	HL-3	1.829	1.785
LH-4	1.632	1.530	HL-4	1.134	1.047
LH-5	0.937	0.921	HL-5	1.135	1.129
LH-6	0.805	0.708	HL-6	0.755	0.678
LH-7	0.695	0.673	HL-7	0.737	0.658
LH-8	1.037	0.847	HL-8	0.853	0.713
LHL-1	1.039	0.787	HLH-1	0.828	0.705
LHL-2	1.354	1.102	HLH-2	1.633	1.402

3.4 Fractographic analysis

Fractographic analysis shows the morphology generated by the fracture of a material or member, and contains fatigue fracture information. Fatigue fractures have characteristics that differ significantly from those of any other type of fracture because they are influenced by properties of the material and stress states. Fractographic images of three typical bolt fractures (LH-5, HL-7, and HLH-2) were obtained by an electron microscope (TESCAN Mira3, LMH) for analysis of the fatigue failure mechanisms (Figs. 11-14).

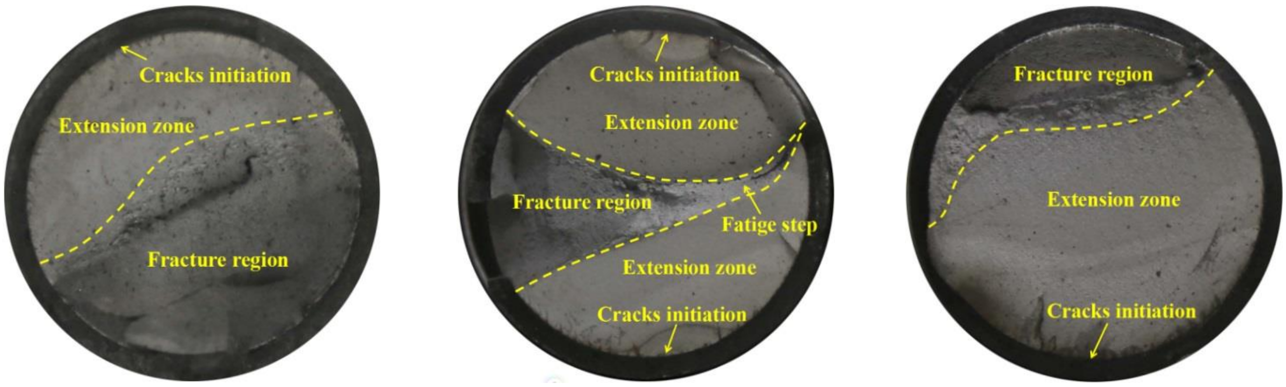

(a) LH-5 (b) HL-7 (c) HLH-2

Fig. 11 Macroscopic view of fatigue fractures

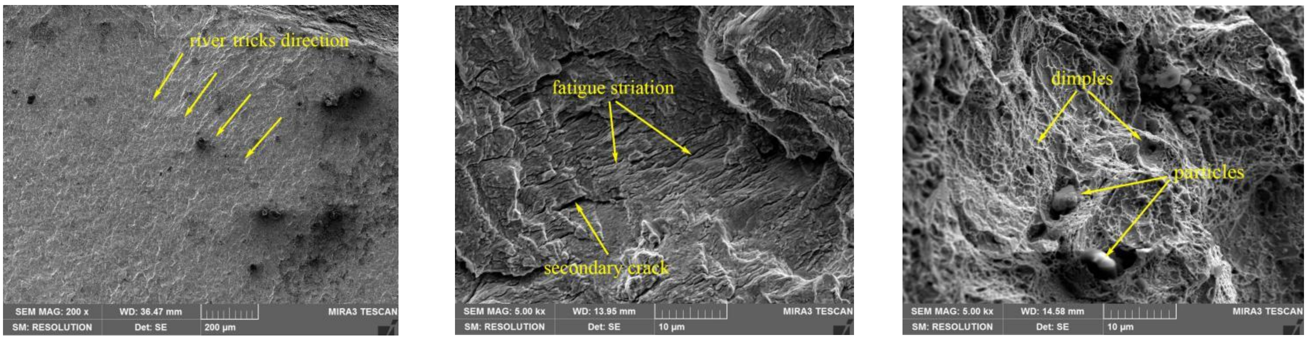

(a) Crack initiation region (b) Crack propagation region (c) Instant fracture region

Fig. 12 Fracture morphology of LH-5

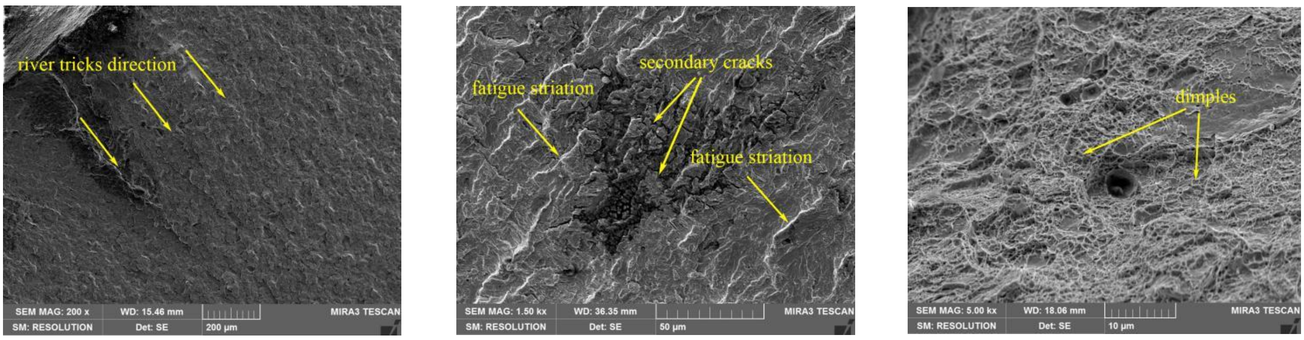

(a) Crack initiation region (b) Crack propagation region (c) Instant fracture region

Fig. 13 Fracture morphology of HL-7

The effect of loading history on the macro-morphology of fatigue fractures can be seen in Fig. 11. LH-5 experienced two load stages corresponding to a stress range from 190 MPa to 200 MPa. The mean stress applied to LH-5 is high, thus crack initiation would occur at a certain point on or near the surface where the stress concentration was highest. Fig. 11(a) shows that the fatigue source is located on the upper left thread. The cracks begin to extend to the center when the crack propagation rate is greater for the high amplitude cycles. In contrast with LH-5, HL-7 experienced four loading stages with stress ranging from 110 MPa to 80 MPa in decrements of 10 MPa when the mean loading stress was lower. Fig. 11(b) shows that the fatigue fracture has two sources: one located on the upper thread and the other located on the lower thread. This is due to strain hardening, which can occur at a lower stress amplitude, causing dislocation movement and subsequent dislocations. As the density of dislocations increases, there will be more interactions between dislocations, and then they will become pinned or tangled. After a large number of lower amplitude loadings, dislocations accumulate and form persistent slip bands PSBs (Suresh 2006), which are small areas where dislocations accumulate and move the surface of the material outward to form steps. These can act as multiple crack initiators (Sarkar *et al.* 2019). When two sources are not on the same plane, a fatigue step is formed

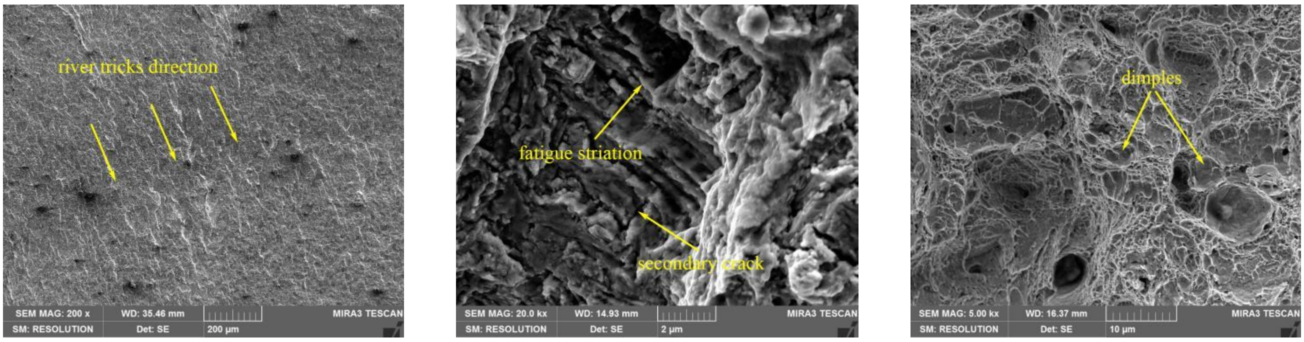

(a) Crack initiation region (b) Crack propagation region (c) Instant fracture region

Fig. 14 Fracture morphology of HLH-2

at the intersection of the crack extensions. Because the crack propagation rate is low during low stress amplitude, the extension zone is very flat and smooth. HLH-2 went through seven load stages, with stress ranging from 110 MPa to 80 MPa to 110 MPa in steps of 10 MPa. Fig. 11(c) shows that the fatigue fracture has only one source located in the lower part. Similarly, because the crack propagation rate is low under low stress loading, it is clear that the crack cross-sections expanded and contracted, and that the continuous extrusion of the metal surface resulted in a flat extension region.

We also found that different loading stresses affected the ratio of the area of the extension zone to the area of the instant fracture region by comparing the final instant fracture regions of the three fracture sections. Fig. 11 shows that the fracture region of LH-5 has the largest area, followed by HL-7 and HLH-2. This is because crack propagation reduces the effective bearing area of the specimen, which causes the stress on the remaining section to gradually increase. The specimen developed an instant fracture when the remaining section was incapable of resisting the stress from the external load. A lower loading stress range leads to a larger area of crack extension but a proportional reduction in the area of instant fractures.

Figs. 12-14 show the typical fatigue failure characteristics of crack initiation, fatigue propagation, and transient fatigue fracture zones. The micro-morphology of the fracture is related to the loading history, but the effect of different load patterns is not so prominent. This may be because the difference in stress range corresponding to each load step is too small, which reduced the effect of sudden stress change on fatigue crack propagation. Figs. 12(a)-14(a) show that the source of fatigue is on the thread root surface where the stress concentration was highest. Each fatigue source zone is relatively smooth and has a deep color, showing river-like patterns toward the inside of the specimen. In the crack propagation zone, fatigue striations and secondary cracks can be observed. The striations are approximately parallel, and the cracks extend in the same direction as the secondary cracks and are perpendicular to the direction of crack propagation. The distances between fatigue striations differ between loading patterns. For LH, the fatigue striations are spaced narrowly for the case when low load stress amplitude cycles are applied first, whereas those tend to be wider when changed to high stress amplitude cycles, as shown in Fig. 12(b). Conversely, the spacing of fatigue crack propagation bands tends to be from wide to narrow for HL (Fig. 13(b)). For HLH, the change trends of the spacing of the fatigue crack propagation stripes is from wide to narrow to wide (Fig. 14(b)), and the opposite is seen for LHL. In the transient fatigue fracture region (Figs. 12(c)-14(c)), the mixed morphology of fatigue fringes and dimples is observed at the junction of the fatigue crack stable extension zone and the fast extension zone. The presence of a large quantity of dimples is the main microscopic feature of the plastic fracture of metal. Crystal particles can be found in the dimples, and the tear marks of the sudden rupture can be observed.

4. Conclusions

From the combination of variable amplitude fatigue tests, cumulative damage models, and fractographic analysis, we draw the following conclusions:

- Fatigue failure of an M30 high-strength bolt in a bolt-sphere joint tends to occur at the first engaged thread between the bolt and the sphere, where the stress is most concentrated, due to the notch effect caused by an abrupt change in cross-section or to defects caused by the manufacturing treatment of the thread surface.
- We used Miner's rule and the Corten-Dolen model to examine the effects of loading history on cumulative fatigue damage. There are differences between D_M and D_{CD}, but the predictions given by the two models nearly coincide for all bolt specimens. The S-N curve equation of variable amplitude fatigue, based on Miner's rule, was developed with equivalent stress amplitude as the design parameter.
- The effect of loading history was observed on the fracture morphology of all bolt specimens. When low stress amplitude cycles are applied first, multiple crack initiations are liable to occur near the thread surface, and a lower loading stress range leads to a larger area of crack extension but a proportional reduction in the area of instant fractures. Moreover, the spacing of crack propagation bands differs between the loading patterns.

Acknowledgments

This project was supported by the National Natural Science Foundation of China (NSFC) through Grant No. 51578357. The authors also would like to thank the Laboratory of Civil Engineering Structures at Taiyuan University of Technology for their support.

References

ANSI/AISC 360-16 (2010), Specification for Structural Steel Buildings, American Institute of Steel Construction; Chicago, IL, USA.

ASTM E606/E606M-12 (2012), Test method for strain-controlled fatigue testing, West Conshohocken, PA, USA.

Chen, S. (2016), *Principles of Steel Structure Design*, Science Press, Beijing, China.

Corten, H.T. and Dolan, T.J. (1956), "Cumulative fatigue damage", *Proceedings of the International Conference on Fatigue of Metals,* London, UK & New York, USA, September.

Eurocode 3 (2003), Design of Steel Structures-Part 1.9: Fatigue, CEN: European Committee for Standardization; Brussels, Belgium.

Fatemi, A. and Yang, L. (1998), "Cumulative fatigue damage and life prediction theories: a survey of the state of the art for homogeneous materials", *Int. J. Fatigue*, **20**(1), 9-34. https://doi.org/10.1016/S0142-1123(97)00081-9

Feng, S. (2017), "Simulation of fatigue load spectrum and fatigue life estimation of space grid with bolt sphere joint", MSc. Dissertation; Taiyuan University of Technology, China.

Feng, X., Lin, X., Pan, W., Qin, Y. and Huang, B. (1995), "Fatigue performance under suspension crane action of bolt ball grid nodes", *J. Build. Struct.*, **16**(4), 3-12. [In Chinese]

Ferjaoui, A., Yue, T., Wahab, M.A. and Hojjati-Talemi, R. (2015), "Prediction of fretting fatigue crack initiation in double lap bolted joint using Continuum Damage Mechanics", *Int. J. Fatigue*, **73**, 66-76. https://doi.org/10.1016/j.ijfatigue.2014.11.012

GB50017-2017 (2017), Standard for Design of Steel Structures, China Architecture and Building Press; Beijing, China.

GB700-2006 (2006), Carbon structural steels, Standard Press of China; Beijing, China.

GB/T13682-1992 (1992), Axial load fatigue testing for threaded fasteners, Standard Press of China; Beijing, China.

He, L., Akebono, H. and Sugeta, A. (2018), "Effect of high-amplitude loading on accumulated fatigue damage under variable-amplitude loading in 316 stainless steel", *Int. J. Fatigue*, **116**, 388-395. https://doi.org/10.1016/j.ijfatigue.2018.06.045

Ibrahim, R.A. and Pettit, C.L. (2005), "Uncertainties and dynamic problems of bolted joints and other fasteners", *J. Sound Vib.*, **279**(3-5), 857-936. https://doi.org/10.1016/j.jsv.2003.11.064

JG/T 10-2009 (2009), Bolted spherical node of space grid structures, Standard Press of China; Beijing, China.

JGJ7-2010 (2010), Technical Specification for Space Frame Structures, China Architecture and Building Press; Beijing, China.

Kapidžić, Z., Ansell, H., Schön, J. and Simonsson, K. (2016), "Fatigue bearing failure of CFRP composite in bolted joints exposed to biaxial variable amplitude loading at elevated temperature", *Compos. Struct.*, **142**, 71-77. https://doi.org/10.1016/j.compstruct.2016.01.064

Lei, H. and Yin, D. (2008), "Research progress on fatigue of grid structure with suspension cranes", *Space Struct.*, **14**(4), 32-36. [In Chinese]

Mahtabi, M.J., Stone, T.W. and Shamsaei, N. (2018), "Load sequence effects and variable amplitude fatigue of superelastic NiTi", *Int. J. Mech. Sci.*, **148**, 307-315. https://doi.org/10.1016/j.ijmecsci.2018.08.037

Miner, M.A. (1945), "Cumulative damage in fatigue", *J. Appl. Mech.*, **12**(3), 159-164.

Qiu, B., Lin, J., Yang, X. and Lei, H. (2017), "Experimental research on fatigue properties of the M30 high-strength bolt under false twisting", *Sci. Tech. Eng.*, **17**(7), 20-25. [In Chinese]

Sarkar, S., Kumar, C.S. and Nath, A.K. (2019), "Investigation on the mode of failures and fatigue life of laser-based powder bed fusion produced stainless steel parts under variable amplitude loading conditions", *Addit. Manuf.*, **25**, 71-83. https://doi.org/10.1016/j.addma.2018.10.044

Sunder, R. (1979), "A mathematical model of fatigue crack propagation under variable amplitude loading", *Eng. Fract. Mech.*, **12**(2), 155-165. https://doi.org/10.1016/0013-7944(79)90108-5

Suresh, S. (2006), *Fatigue of Materials*, (2nd Edition), Cambridge University Press, Cambridge, UK.

Xu, G. and Cui, J. (1994), "Grid structure fatigue and fatigue life calculation", *J. Build. Struct.*, **15**(2), 25-34. [In Chinese]

Yang, X. (2017), "The theoretical and experimental research on fatigue performance of M30 and M39 high-strength bolts in grid structures with bolt sphere joints", Ph.D. Dissertation; Taiyuan University of Technology, China.

Yang, X. and Lei, H. (2017), "Constant amplitude fatigue test of high-strength bolts in grid structures with bolt–sphere joints", *Steel Compos. Struct., Int. J.*, **25**(5), 571-579. https://doi.org/10.12989/scs.2017.25.5.571

Zhou, S., Sun, Y., Ge, J. and Chen, X. (2015), "Multiaxial fatigue life prediction of composite bolted joint under constant amplitude cycle loading", *Compos. B Eng.*, **74**, 131-137. https://doi.org/10.1016/j.compositesb.2015.01.013

Zhu, H. (2011), "Calculation methods for equivalent fatigue stress amplitude based on Corten-Dolan accumulative damage rule", *Adv. Mater. Res.*,**156-157**, 1271-1274. https://doi.org/10.4028/www.scientific.net/AMR.156-157.1271

Zuo, F., Huang, H., Zhu, S., Lv, Z. and Gao, H. (2015), "Fatigue life prediction under variable amplitude loading using a non-linear damage accumulation model", *Int. J. Damage Mech.*, **24**(5), 767-784. https://doi.org/10.1177/1056789514553042

CC

Appendix A

Table A1 The variable amplitude fatigue test results of M30 high strength bolts

Number	σ_{max} (MPa)	σ_{min} (MPa)	$\Delta\sigma_i$ (MPa)	N_i $(\times 10^4)$	N_f $(\times 10^4)$	Number	σ_{max} (MPa)	σ_{min} (MPa)	$\Delta\sigma_i$ (MPa)	N_i $(\times 10^4)$	N_f $(\times 10^4)$
LH-1	225	135	90	223.37	250.84	HL-1	275	165	110	21.87	190.46
	250	150	100	27.47			250	150	100	168.59	
LH-2	300	180	120	0.47	78.27	HL-2	350	210	140	23.32	26.53
	325	195	130	77.80			325	195	130	3.21	
LH-3	350	210	140	13.72	21.83	HL-3	425	255	170	30	41.58
	375	225	150	8.11			400	240	160	11.58	
LH-4	425	255	170	23.77	33.48	HL-4	475	285	190	2.38	20.15
	450	270	180	9.71			450	270	180	17.77	
LH-5	475	285	190	2.89	12.71	HL-5	525	315	210	12.05	12.92
	500	300	200	9.82			500	300	200	0.87	
LH-6	225	135	90	30.00	88.36	HL-6	275	165	110	30.00	79.15
	250	150	100	30.00			250	150	100	30.00	
	275	165	110	28.36			225	135	90	19.15	
LH-7	200	120	80	30.00	97.95	HL-7	275	165	110	30.00	80.60
	225	135	90	30.00			250	150	100	30.00	
	250	150	100	30.00			225	135	90	7.12	
	275	165	110	7.95			200	120	80	13.48	
LH-8	225	135	90	30.00	102.31	HL-8	300	180	120	11.20	78.32
	250	150	100	30.00			275	165	110	30.00	
	275	165	110	25.20			250	150	100	30.00	
	300	180	120	17.11			225	135	90	7.12	
LHL-1	200	120	80	30.00	123.08	HLH-1	250	150	100	30.00	98.68
	225	135	90	30.00			225	135	90	30.00	
	300	180	120	11.20			200	120	80	13.48	
	250	150	100	30.00			275	165	110	25.20	
	275	165	110	21.88		HLH-2	275	165	110	31.31	192.34
LHL-2	200	120	80	30.00	174.48		250	150	100	30.00	
	225	135	90	30.00			225	135	90	19.15	
	250	150	100	30.00			200	120	80	30.00	
	275	165	110	23.94			225	135	90	30.00	
	250	150	100	30.00			250	150	100	30.00	
	225	135	90	30.54			275	165	110	21.88	

Appendix B

Table B1 The constant amplitude fatigue test results of M30 high strength bolts

Number	σ_{max} (MPa)	σ_{min} (MPa)	$\Delta\sigma$ (MPa)	N_f $(\times 10^4)$	Number	σ_{max} (MPa)	σ_{min} (MPa)	$\Delta\sigma$ (MPa)	N_f $(\times 10^4)$
M30-1	225	135	90	264.35	M30-20	400	240	160	19.55
M30-2	225	135	90	160.89	M30-21	400	240	160	28.06
M30-3	225	135	90	120.45	M30-22	400	240	160	21.67
M30-4	250	150	100	195.87	M30-23	425	255	170	18.78
M30-5	250	150	100	105.40	M30-24	425	255	170	18.92
M30-6	250	150	100	105.60	M30-25	425	255	170	35.43
M30-7	275	165	110	126.90	M30-26	450	270	180	21.26
M30-8	275	165	110	116.98	M30-27	450	270	180	14.94
M30-9	275	165	110	69.16	M30-28	450	270	180	14.38
M30-10	300	180	120	71.13	M30-29	475	285	190	12.09
M30-11	300	180	120	53.55	M30-30	475	285	190	18.20
M30-12	325	195	130	38.88	M30-31	475	285	190	11.38
M30-13	325	195	130	42.13	M30-32	500	300	200	17.42
M30-14	350	210	140	38.57	M30-33	500	300	200	17.88
M30-15	350	210	140	28.97	M30-34	500	300	200	9.41
M30-16	375	225	150	23.77	M30-35	525	315	210	13.83
M30-17	375	225	150	39.90	M30-36	525	315	210	11.61
M30-18	375	225	150	23.17	M30-37	525	315	210	16.82
M30-19	400	240	160	33.13					